Trichel-like Pulses in Negative Corona Discharge Under a Supersonic Flow

Guillaume Dufour, Konstantinos Kourtzanidis, François Rogier

AIAA AVIATION Forum
12-16 June 2023, San Diego, CA and Online
AIAA AVIATION 2023 Forum

10.2514/6.2023-4026

Trichel-like pulses in negative corona discharge under a supersonic flow

G. Dufour* and F. Rogier†
ONERA/DTIS, Université de Toulouse, France

K. Kourtzanidis‡
CERTH - Centre for Research and Technology Hellas, 57001 Thermi, Thessaloniki, Greece

We propose a self-consistent, transient numerical study of negative corona discharges produced in front of a blunted body in a supersonic Mach 3 flow. Taking into account the supersonic flow field and the bow shock wave formation which includes variable gas temperature, density and velocity distribution, the plasma discharge dynamics is analyzed, revealing high frequency discharge pulses similar to typical Trichel pulses in point-to-plane, known to exist in atmospheric discharges without or with low-speed external flow, although the process giving birth to these pulses is completely different. Through numerical simulations we show how, after a first strong ionization phase happened in front of the blunt body, the supersonic flow field acts on the ionic species displacements and changes the local charge distribution so that a new ionization phase can take place. In order to assess more precisely this effect, a panel of numerical test-cases are proposed with different transport velocities of the charged species by the supersonic flow.

I. Nomenclature

D_1	=	Total diameter of the actuator
D	=	Dielectric diameter
d	=	Anod (spike) diameter
Ls	=	Anod length
e	=	Dielectric gap
n_s	=	Density number of species s
v_s	=	Velocity of species s
q_s	=	Charge of species s
Γ_s	=	Flux of species s
μ_s	=	Mobility of species s
D_s	=	Diffusion coefficient for species s
u	=	Gas velocity
E	=	Electric field
Φ	=	Electric potential
ρ	=	Local charge
ε	=	Local permittivity
S_s	=	Net rate of production of species s
$c_{s,r}$	=	Net number of particles of species s created or lost in one reaction of type r
R_r	=	Rate of the reaction of type r

II. Introduction

Supersonic flow control at high altitude is a real challenge for increasing the performance of military and civil aircraft. Experiments to stabilize an unsteady Mach 3 shock wave on a truncated body fitted with a central spike

*Research Engineer, ONERA/DTIS, 2 av. E. Belin 31400 Toulouse, France
†Research Engineer, ONERA/DTIS, 2 av. E. Belin 31400 Toulouse France
‡Research Engineer, CERTH - Centre for Research and Technology Hellas, 57001 Thermi, Thessaloniki, Greece

have showed the existence of a pulsed regime for the discharge [1, 2], but the physical explanation of the mechanism of interaction between the plasma and the incoming flow remains not well understood. The existence of Trichel pulses for negative point-to-plane discharge in quiescent atmosphere is a well-known phenomenon, which has been experimentally investigated [3, 4]. In [3], Zhang et al. explain that a Trichel pulse is a mode transition between the low-current Townsend and high current glow regime. In their paper, they emphasize the fact that the positive ions play a major role for the pulse formation. In this work, we perform a modelling and numerical simulation of the experiment carried out in [2] using an in-house 2D-axisymmetric fluid plasma code, COPAIER, whose ability to simulate plasma discharge has already been demonstrated [5, 6]. We use the knowledge of the resulting positive ions density profile in order to explain the existence of Trichel-like pulses. A first numerical simulation of this experiment has already been performed using a quasi-neutral plasma model and showed no pulse [7]. This study highlights the impact of the supersonic flow on both the positive and negative ions density profile as well as on the discharge dynamics, unlike what is observed in low-speed configurations, and shows the existence of a pulsed regime for the discharge current.

III. Experimental setup and numerical modelling

A. Experimental setup

We are interested in modelling the experiment run by P.-Q. Elias as described in [1, 2]. The actuator uses a 2D-axisymmetric geometry and consists of a spike (the anode, located along the symmetry axis) and two grounded electrodes located along a dielectric material. The scheme of the actuator is represented on Figure 1 (left).

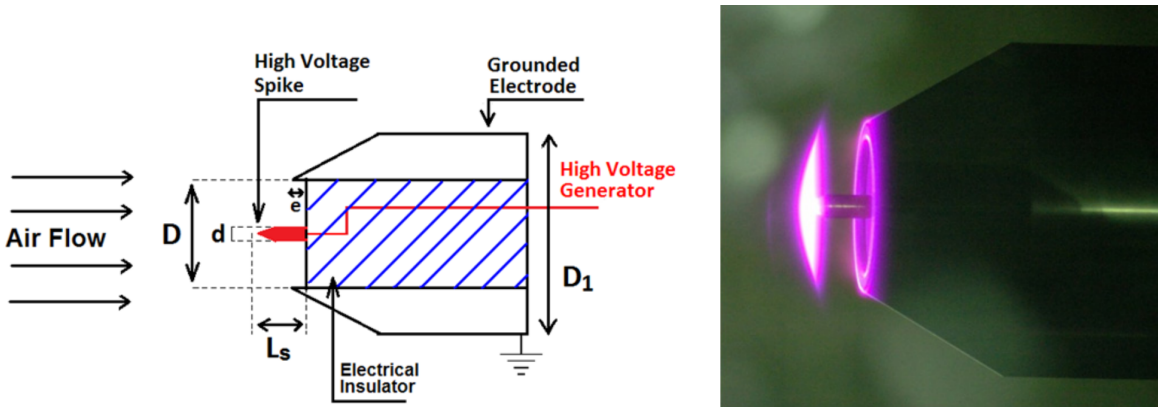

Fig. 1 Schematic diagram of experimental setup (left) and actuator with plasma turned on (right) [1]

The actuator operates under an incoming supersonic flow and the plasma discharge interacts with the flow, exhibiting an umbrella shaped glow as shown on Figure 1 (right). All dimensions and characteristics of the actuator are given in Table 1.

Table 1 Geometric values for the actuator

D_1	D	d	Ls	e
70 mm	35 mm	5 mm	14 mm	2 mm

B. Plasma model

The plasma discharge has been simulated using an in-house plasma-fluid numerical solver, COPAIER [5, 6]. The physical model is based on a self-consistent, multi-species, and multi-temperature continuum (fluid) description of the plasma. Each of the species, s, considered in the pre-defined plasma-gas chemistry is governed by a continuity equation:

$$\frac{\partial n_s}{\partial t} + \mathrm{div}(\Gamma_s) = S_s \qquad \text{with } S_s = \sum_r c_{s,r} R_r \tag{1}$$

where n_s is the density number of species s, S_s is the net rate of production of species s due to chemical reactions, $c_{s,r}$ is the net number of particles of species s created or lost in one reaction of type r (so it can be positive or negative). The reaction rate R_r is proportional to the densities of the reacting species, with a reaction rate coefficient depending on the reaction and the Townsend coefficient.

The species number flux is given by the momentum balance equation, which is approximated by the drift-diffusion equation:

$$\Gamma_s = n_s v_s, \qquad \Gamma_s = \mathrm{sgn}(q_s) n_s \mu_s E - D_s \nabla(n_s) - n_s u \tag{2}$$

where q_s is the species charge, μ_s and D_s are the species mobility and diffusion coefficient respectively, and u is the mean mass fluid convection velocity. The electric field is defined as deriving by a potential solving the Poisson equation:

$$E = -\nabla\Phi, \qquad \mathrm{div}(\varepsilon\nabla\Phi) = -\rho = -\sum_s q_s n_s \tag{3}$$

where ε is the dielectric permittivity. In equation (2) , the diffusion coefficient is related to the mobility term by Einstein's relation. The rest of transport (mobility μ) and reaction rate coefficients are tabulated with an electric field dependence under the Local Field Approximation (LFA) which assumes a direct relation between the species energy distribution, the electric field and the surrounding flow characteristics (density, temperature, etc.). Such dependence is known through either experiments, theory or direct solution of the Boltzmann equation. This approximation has been demonstrated to be consistent with the regime of corona discharges such as the one studied in [8].

In order to save computational time, we choose to use a simplified air-plasma chemistry, reduced to three different charged species, as described in Table 2. Boeuf et al. [9] have shown that such chemistry allows for a proper description of the main charged species production, discharge evolution and qualitative EHD force production while largely reducing the CPU burden of the simulation. To determine the values for transport and reaction rate coefficients, some assumptions have been made: air is mostly composed of dioxygen and nitrogen (with respective proportions 20% and 80%), negatives ions are exclusively O^- , and positive ions are either N^+ or O^+. All values have been computed using the BOLSIG+ solver [10] under the Local Field Approximation (LFA) assumption.

Table 2 Air / Plasma chemistry

4 species	Electrons (e) Positive ions (ip) Negative ions (in) Neutrals (n)
5 reactions	Ionization : e + n $\rightarrow$ 2e + ip 2-body attachment : e + n $\rightarrow$ in 3-body attachment : e + 2n $\rightarrow$ in + n Electron-ion recombination : e + ip $\rightarrow$ n Ion-ion recombination : in + ip $\rightarrow$ 2n

C. Mesh and incoming flow

The solver COPAIER uses structured or unstructured 2D or 2D-axisymmetric meshes. For our simulations, an unstructured mesh was generated using GMSH [11], with a strong refinement close to the anode. This mesh is represented on Figure 2 and allows for a precise computation of the electric field, even near the anode.

In total, the mesh includes 123, 434 elements (triangles) and 64, 626 points. The characteristic length associated to the smallest elements is about one micrometer, which corresponds to the minimum values of the Debye length reached during the simulation.

In order to calculate the values of the mobility and reaction coefficients and to have the value of the surrounding flow u appearing in equation (3), we have performed a computation of the incoming flow profile using the solver OpenFOAM [12]. The computation has been performed with the discharge being turned off, we assume in this study

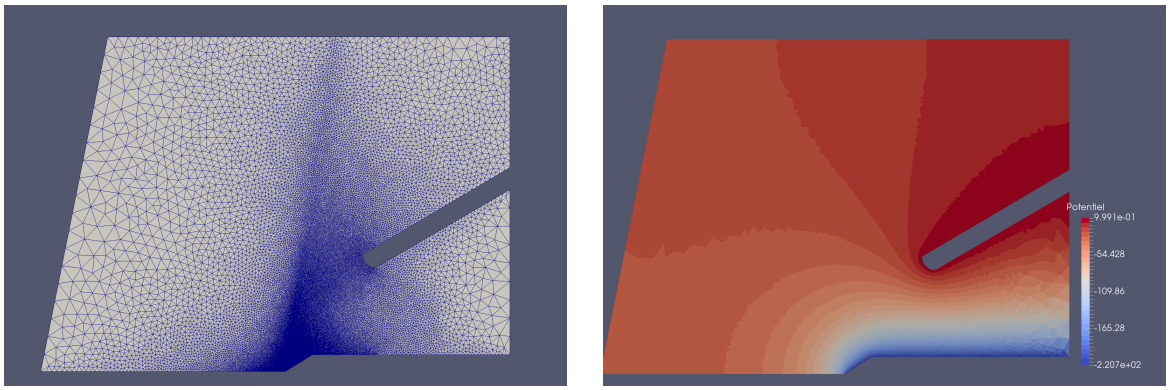

Fig. 2 Mesh refinement (left) and computed electrostatic potential ([V/m], right) obtained with COPAIER

that we have a one-way coupling between the discharge and the flow. To avoid errors due to an interpolation process between COPAIER and OpenFOAM, both solvers used the same mesh.

Table 3 Incoming flow characteristics

Parameter	Description	Value
P	Upwind pressure	3000 Pa
T	Upwind temperature	120 K
Re	Reynolds number	1.08E7
V	Upwind velocity	680 m.s^{-1}
M	Mach number	3.1

All the conditions of the flow simulation are gathered in table 3 while Figure 3 reveals the corresponding density and velocity profiles, showing the shockwave generated by the spike (the anode) of the actuator.

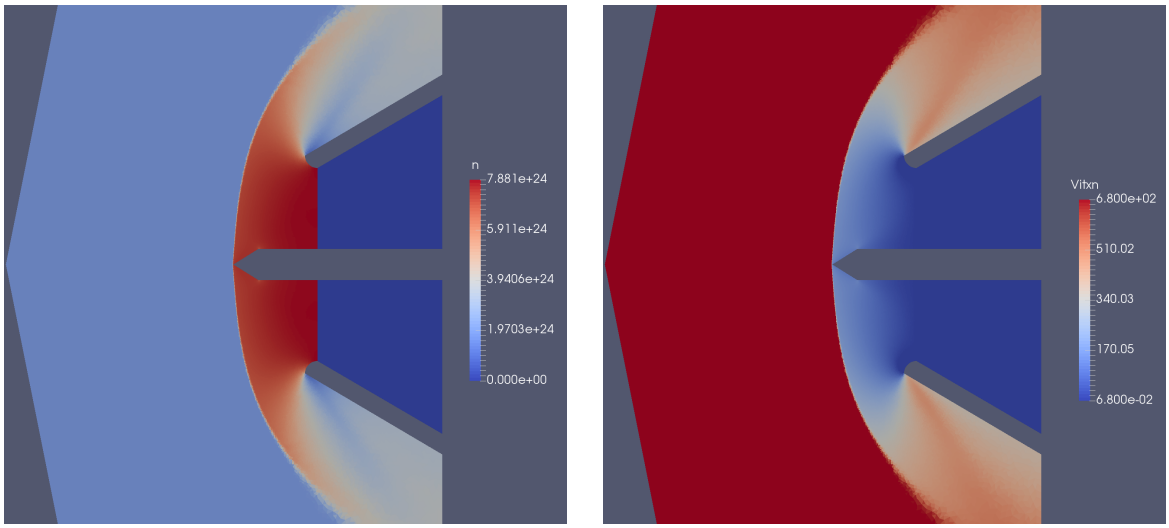

Fig. 3 Density (left) and axial velocity (right) profiles obtained with OpenFOAM

As for the applied potential, a ramp of potential has been used: the applied potential changes linearly from 0V to the target value in one microsecond. All the computations were performed on a parallel cluster at ONERA, using the MPI paradigm. The initial mesh was split into 32 domains, each comprising roughly the same number of cells. A node in the cluster consists of two Intel(R) Xeon(R) CPU E5-2650 v4, running at 2.2GHz, each one having 12 cores (30 MB L3).

IV. First numerical results and pulse dynamics

A. Discharge current

We present in this section the discharge dynamics obtained for three different applied voltage values, namely −7.5 kV, −8.5 kV and −9.5 kV. Figure 4 shows the discharge current obtained for this three operating conditions, for a physical time up to 150 milliseconds for the −7.5 kV while the other two simulations were stopped at 65 milliseconds. After an initial peak of current (not shown here as it skews the graphics and only due to the fact that the initial condition is assumed to be a constant, charge neutral state over the whole domain), a quasi-periodic behavior is reached for all three voltage values. The behavior consists in regular pulses of current, it can be noticed that the three discharges follow the same trend. While the amplitude grows with the applied voltage absolute value, the frequency of the pulses does not seem to be modified by the applied voltage.

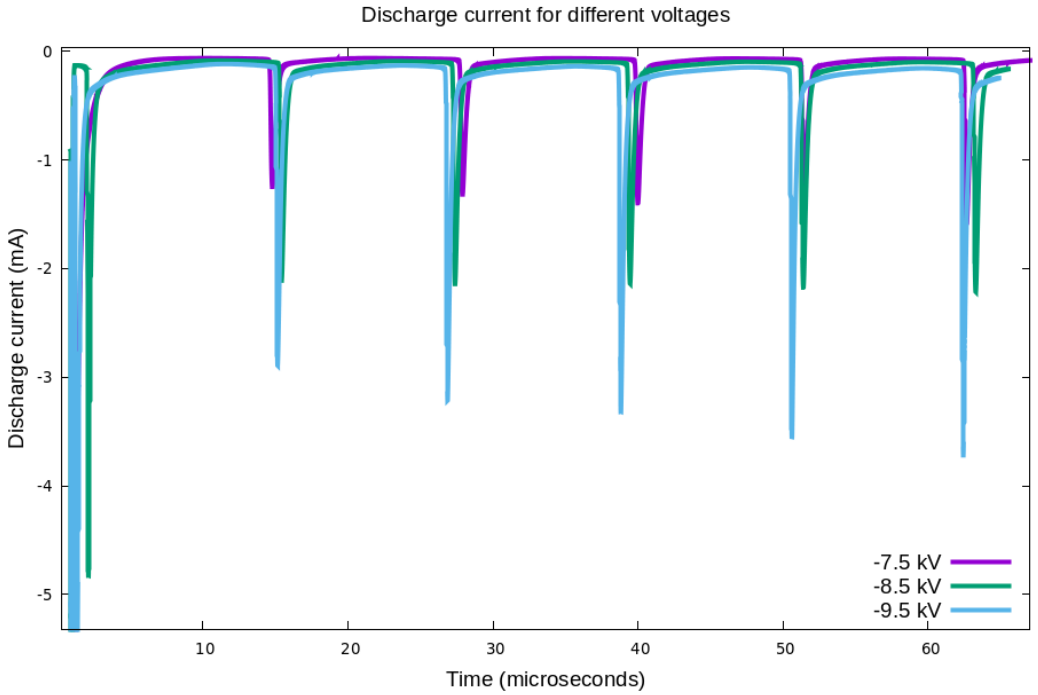

Fig. 4 Discharge current in the periodic regime for all three applied voltages

Table 4 collects both the amplitude of each pulse and the duration between the pulse and the preceding one, once the quasi-periodic state is reached, for the −7.5 kV discharge. We can then estimate the frequency of these pulses.

Table 4 Pulse characteristics for the -7.5 kV discharge

Pulse number	**2**	**3**	**4**	**5**	**6**	**7**	**8**	**9**	**10**
Duration (μs)	13.11	12.09	11.45	11.22	11.30	11.54	11.74	11.90	11.90
Frequency (Hz)	76.28	82.71	87.34	89.12	88.5	86.66	85.18	84.03	84.03
Intensity (mA)	−1.32	−1.40	−1.49	−1.59	−1.63	−1.61	−1.61	−1.57	−1.56

The existence of this kind of pulses, known as Trichel pulses, has already been observed in the literature for negative point-to-plan discharges in air. Tran et al. [4] performed a study of the frequency of these pulses depending on operating conditions (secondary emission coefficient, applied voltage, etc.) and showed that these frequencies vary between 60 and 200 kHz while the maximum measured value for the discharge current range between 1 and 3 mA. While our simulation stay in the range of these values, we show that the pulses are triggered by a different phenomenon than in [4].

B. Positive ions density profiles

The main difference between the experiments in [4] and our simulation, apart the shape of the actuator, is that the velocity of the surrounding flow is of the same order of magnitude than the velocity of the ions due to the presence of the electric field. Figure 5 shows the evolution of the positive ions density profile during the first four pulses. It reveals that when a pulse occurs, a lot of positive ions (and also negative ions, not represented here) are generated through ionization. The electrostatic field is screened by the local charge field and this generation stops. Then, these ions are transported by the incoming flow, the screening ends and a new pulse can occur.

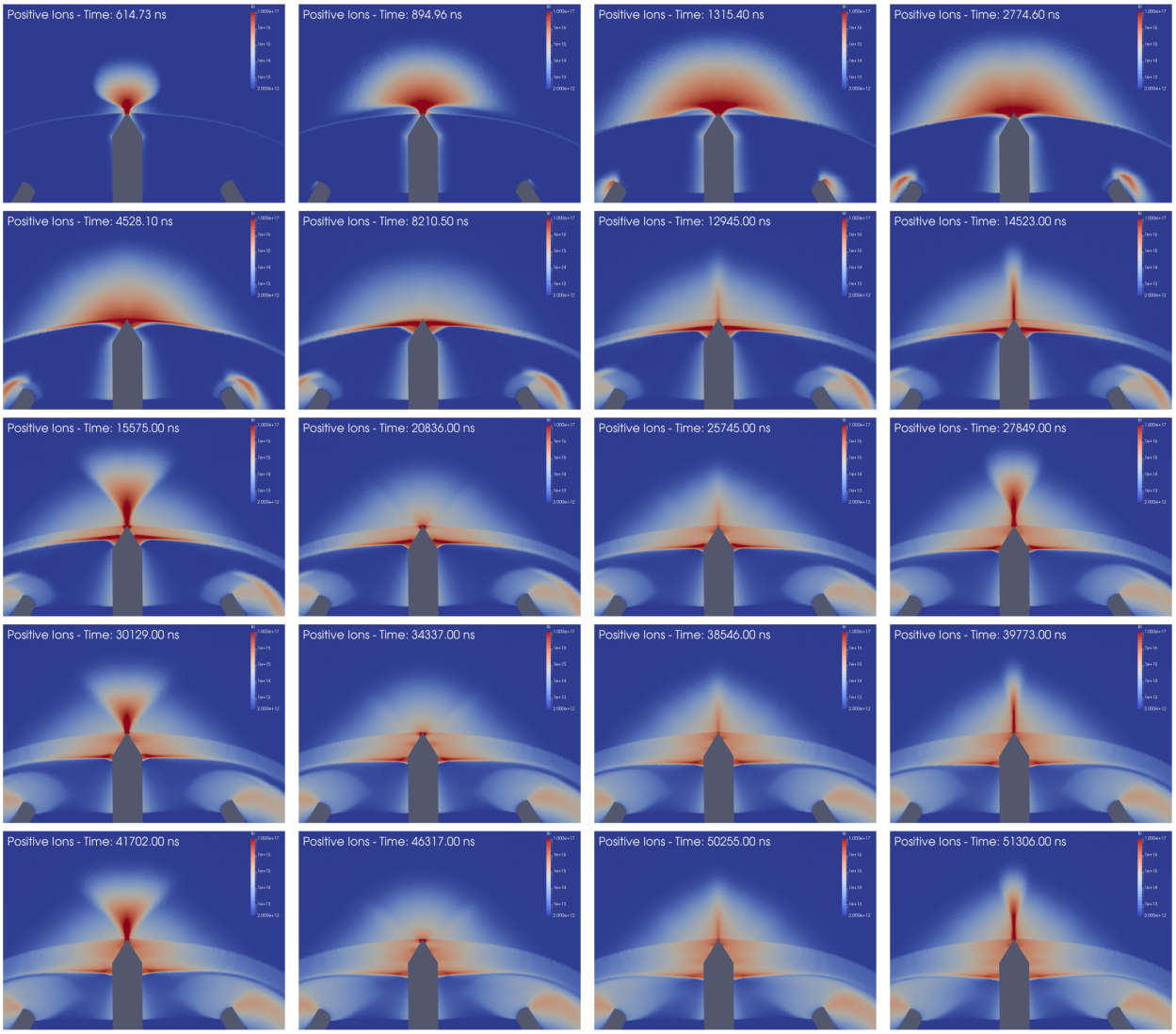

Fig. 5 Positive ion density profiles for the first four pulses (logarithmic scale)

V. Assessing the effect of the supersonic flow on the discharge dynamics

A. A set of numerical test-cases

We will propose in this section a series of numerical tests to further study the effect of the incoming flow velocity on the discharge dynamics. In order to focus on the velocity parameter, we define a specific flow profile: the density and pressure profiles are unchanged from the previous simulation while the transport velocities (both axial and radial) seen by the charged species in the code (parameter u in equation 2.2) have been scaled with a factor α. We the have the new

equation for the flux Γ_s:

$$\Gamma_s = n_s v_s^{\alpha}, \qquad \Gamma_s = \mathrm{sgn}(q_s) n_s \mu_s E - D_s \nabla(n_s) - n_s \alpha u \tag{4}$$

A total of seven simulations are conducted with scale factors α ranging from 1 (reference simulation) to 0 (no transport of the charged species by the incoming flow considered), with intermediate values $\alpha = 0.9$, 0.7, 0.4, 0.3 and 0.2. In order to limit the effect of the initial current peak of the discharge and to save computational time, all the simulations use the same initial condition, which is given by the state of the discharge obtained in the previous simulation at time $t = 150\mu$s. In all these simulations, the applied potential value is set to −9.5 kV.

B. Effects on the discharge current

Figure 6 shows the discharge current obtained under these conditions for the scaling factors 1, 0.9, 0.7 and 0.4. After a first pulse due to the sudden change of the velocity for the charged species (not represented on the figure for readability), the pulsed regime is preserved but with reduced amplitude and frequency as the scaling factor decreases.

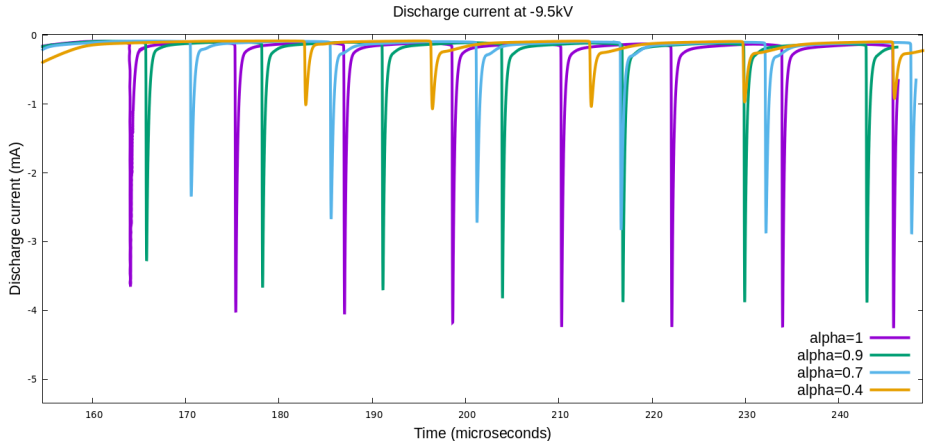

Fig. 6 Discharge current for scaling factors $\alpha = 1$, 0.9, 0.7 and 0.4.

On figure 7 is represented the discharge current for the scaling factors 0.4, 0.3, 0.2 and 0.0.

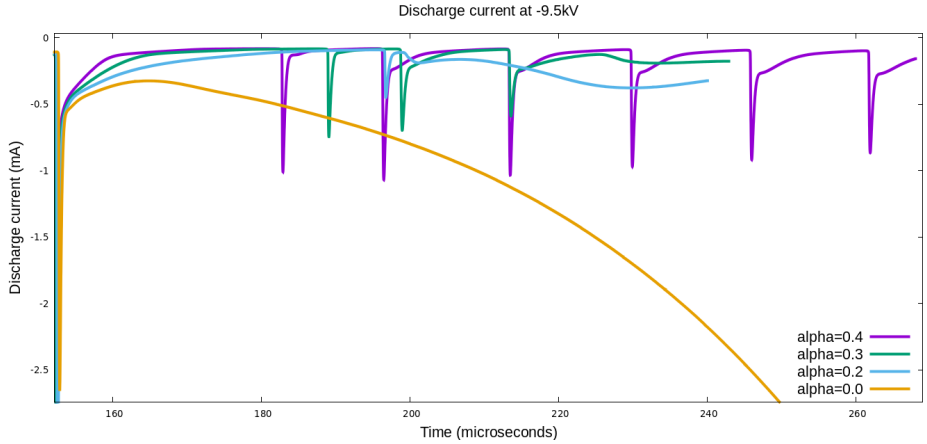

Fig. 7 Discharge current for scaling factors $\alpha = 0.4$, 0.3, 0.2 and 0.0.

It can be seen that the monotonic trend observed on figure 6 with respect to the scaling factor is no longer preserved with a scaling factor less than 0.4, the behavior of the current shows some changes and the current does converge towards a stationary value. This value for $\alpha = 0.0$ being quite large with respect to the other two, the plot has been

cropped. It can be noted that in order to confirm that the pulsed regime sill holds for $\alpha = 0.4$ and does not vanish two additional pulses were simulated for this figure.

To summarize, the scaling on the surrounding flow velocity acts on both the amplitude and the frequency of the observed pulses. The amplitude and the frequency of the pulses follows a monotonic trend (the slower the impact of the flow, the lower the amplitude and the frequency). These values have been compiled in table 5, when no pulsed regime exists (NP), the intensity is the limit value for the discharge current.

Table 5 Pulse characteristics for the -9.5 kV discharge

Scaling factor	**1.0**	**0.9**	**0.7**	**0.4**	**0.3**	**0.2**	**0.0**
Duration (μs)	11.80	13.20	15.51	16.11	NP	NP	NP
Frequency (Hz)	84.74	75.75	64.47	62.12	NP	NP	NP
Intensity (mA)	−4.01	−3.83	−2.82	−0.95	−0.175	−0.317	−5.21

This behavior can be interpreted by the ability (or not) of the surrounding flow to displace the ionic species so that the screening of the electrostatic field by the discharge is nullified and allows for a new pulse. In order to confirm this hypothesis we will look at the dynamics of the charged species density profile and illustrate how the flow interact with them.

C. Ions density profiles

We present here the impact of the scaling factor on the positive and negative ions density profiles. We recall that the initial velocity profile shown on figure 3 for the surrounding flow is about 680 m.s^{-1} just before the tip of the electrode and between 100 and 300 m.s^{-1} just after the tip. This value is of the same order of magnitude than the drift velocity of the charged species in the electric field near the tip of the stressed electrode just after a pulse (see figure 8).

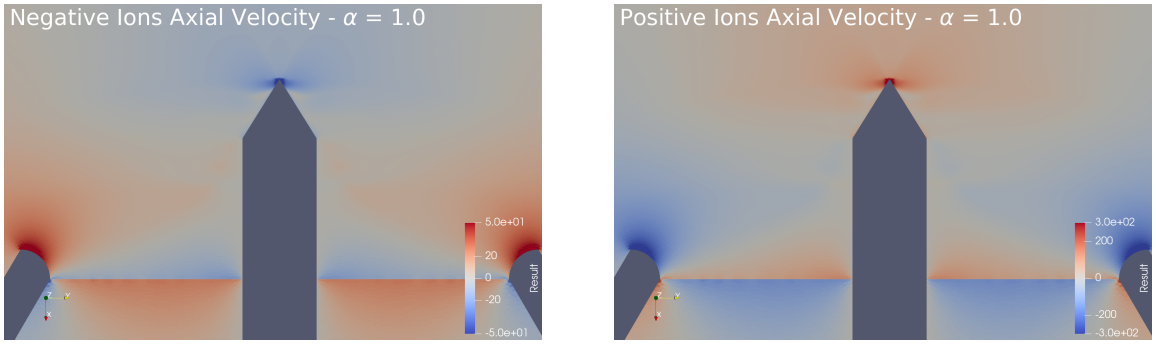

Fig. 8 Negative (left) and positive (right) ions drift velocities near the tip of the stressed electrode ($\alpha = 1.0$)

Since the flow is going towards the tip of the stressed electrode, positive value of the velocities correspond to ions going from the top to the bottom of the figure. We can then observe that the negative ions would be moving upstream of the incoming flow if they were only subject to the drift in the electrical field.

The different negative ions density profiles obtained for different values of α are represented on figure 9, showing clearly the effect of the flow on the density profile. For high values of α, the negative ions remain close to the stressed electrode and are pushed towards the base of the device, which is the result of adding the transport of the incoming flow to the drift in the electric field. When the effect of the incoming flow is reduced (low values of α), a different shape is obtained for the density profile, with an area of high density remaining stable upstream of the electrode. In this case, the electric field remains partially shielded and no pulse is created, which is consistent with the discharge current profile.

The different positive ions density profiles obtained for different values of α are represented on figure 10, showing two different types of structures. For the first one, corresponding to a high effect of the surrounding flow comparable to the drift velocity of the charged species, a mechanism similar to the one described in section IV, part B takes place. We can observe a series of areas of higher densities which have been created during a pulse and were pushed away from the tip of the electrode by both the surrounding flow and the electric field. On the contrary, when the scaling factor

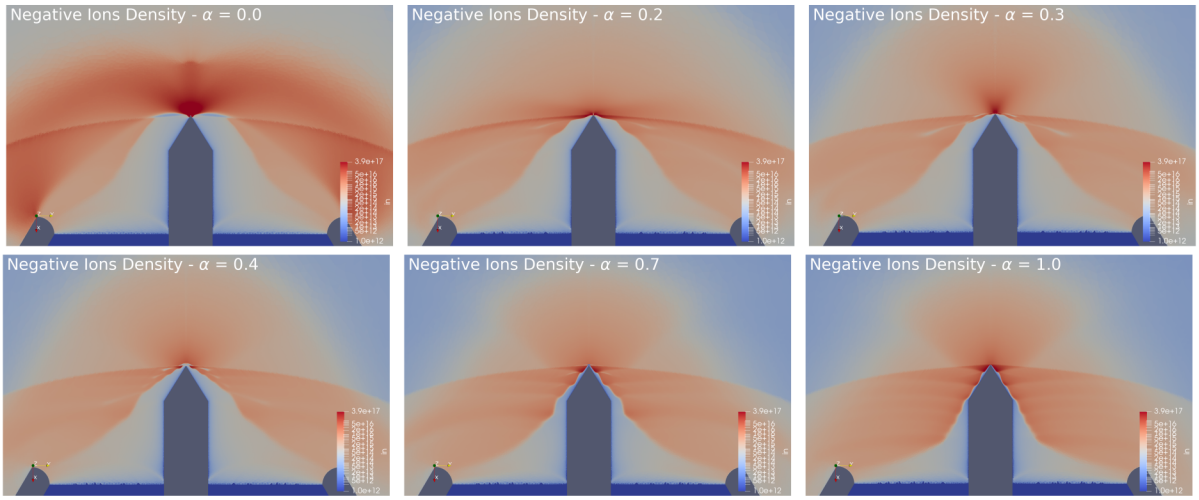

Fig. 9 Negative ions density profiles for different scaling factors

decreases and the effect of the flow velocity is not important enough there is a change of structure, the profile of the charged species densities tends to become stable after a first spike and the pulsed regime disappears

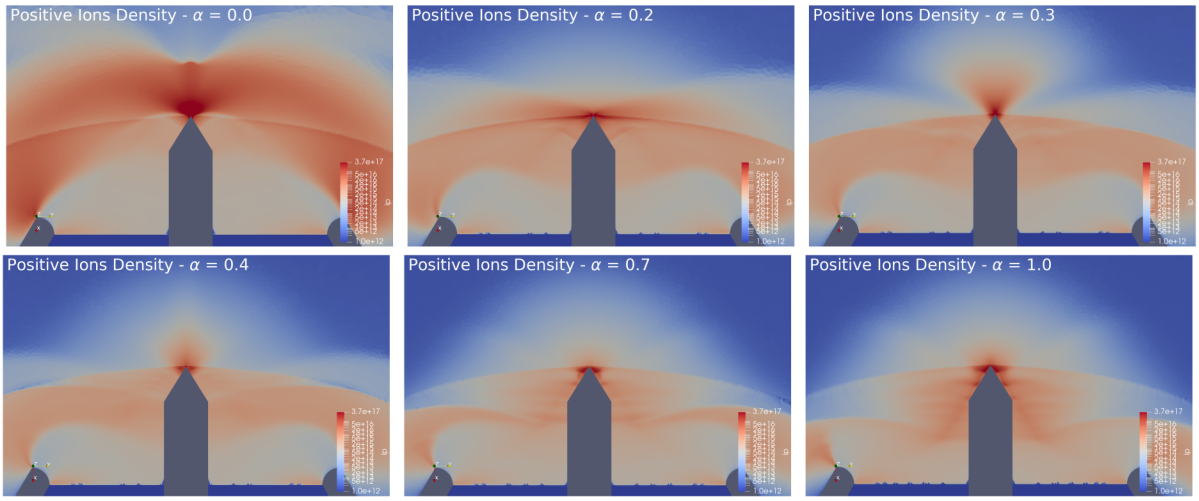

Fig. 10 Positive ions density profiles for different scaling factors

VI. Conclusion

We proposed a simulation of a negative corona discharge under a supersonic flow and showed the existence of Trichel-like pulses for the discharge current. Through the use of numerical simulations of these plasma discharges under artificial effects for the surrounding flow, we could exhibit the mechanism creating these pulses which is entirely relying on the effect of the supersonic flow, acting on the distribution profiles of the charged species if its velocity is comparable to the drift velocity of the charged species in the electric field. In that case, the role of the negative ions density profile seems dominating. This also emphasizes the need to take into account the charge separation in the simulation of the discharge so that quasi-neutral approximations may not be suited to simulate this kind of setup.

As for the interactions between the discharge and the flow, this study has been made under a one-way assumptions and the effects of the discharge on the flow (source of momentum, heat) have been neglected. Future works should focus on lifting this assumption and study the fully coupled effect since our results indicate that the discharge may be very dependant on the flow profile near the electrode. Another point of interest will be to raise the voltage applied to the

electrode and try to capture the change of discharge regime that is described in [2].

References

[1] Elias, P.-Q., Chanetz, B., Larigaldie, S., and Packan, D., "Study of the effect of glow discharges near a M= 3 bow shock," *AIAA journal*, Vol. 45, No. 9, 2007, pp. 2237–2245.

[2] Elias, P.-Q., Chanetz, B., Larigaldie, S., Packan, D., and Laux, C., "Mach 3 shock wave unsteadiness alleviation using a negative corona discharge," *AIAA journal*, Vol. 46, No. 8, 2008, pp. 2042–2049.

[3] Zhang, Y., Xia, Q., Jiang, Z., and Ouyang, J., "Trichel pulse in various gases and the key factor for its formation," *Scientific reports*, Vol. 7, No. 1, 2017, pp. 1–8.

[4] Tran, T., Golosnoy, I., Lewin, P., and Georghiou, G., "Numerical modelling of negative discharges in air with experimental validation," *Journal of Physics D : Applied Physics*, Vol. 44, No. 1, 2010.

[5] Dufour, G., and Rogier, F., "Numerical Modeling of Dielectric Barrier Discharge Based Plasma Actuators for Flow Control: the COPAIER/CEDRE Example," *AerospaceLab*, 2015.

[6] Kourtzanidis, K., Dufour, G., and Rogier, F., "The electrohydrodynamic force distribution in surface AC dielectric barrier discharge actuators: do streamers dictate the ionic wind profiles?" *Journal of Physics D: Applied Physics*, Vol. 54, No. 26, 2021, p. 26LT01.

[7] Rassou, S., Packan, D., Elias, P.-Q., Tholin, F., Chemartin, L., and Labaune, J., "Numerical modeling of a glow discharge through a supersonic bow shock in air," *Physics of Plasmas*, Vol. 24, No. 3, 2017, p. 033509.

[8] Kourtzanidis, K., Dufour, G., and Rogier, F., "Self-consistent modeling of a surface AC dielectric barrier discharge actuator: in-depth analysis of positive and negative phases," *Journal of Physics D: Applied Physics*, Vol. 54, No. 4, 2020, p. 045203.

[9] Boeuf, J., Lagmich, Y., Unfer, T., Callegari, T., and Pitchford, L., "Electrohydrodynamic force in dielectric barrier discharge plasma actuators," *Journal of Physics D: Applied Physics*, Vol. 40, No. 3, 2007, p. 652.

[10] "Bolsig+ version 12/2017 accessed online," , 2017.

[11] Geuzaine, C., and Remacle, J.-F., "Gmsh: A 3-D finite element mesh generator with built-in pre-and post-processing facilities," *International journal for numerical methods in engineering*, Vol. 79, No. 11, 2009, pp. 1309–1331.

[12] Chen, e. a., Goong, "OpenFOAM for computational fluid dynamics." *Notices of the AMS 61.4*, 2014, pp. 354–363.